Journal of Materials Chemistry C

Pressure-induced suppression of charge density phases across the entire rare-earth tritellurides by optical spectroscopy

Journal:	*Journal of Materials Chemistry C*
Manuscript ID	TC-ART-05-2022-002137.R1
Article Type:	Paper
Date Submitted by the Author:	18-Jul-2022
Complete List of Authors:	Kopaczek, Jan; Arizona State University, School for Engineering of Matter, Transport and Energy; Wroclaw University of Science and Technology, Department of Semiconductor Materials Engineering Li, Han; Arizona State University, School for Engineering of Matter, Transport and Energy Yumigeta, Kentaro; Arizona State University, School for Engineering of Matter, Transport and Energy Sailus, Renee ; Arizona State University, School for Engineering of Matter, Transport and Energy Sayyad, Mohammed Y. ; Arizona State University, School for Engineering of Matter, Transport and Energy Moosavy, Seyed Tohid Rajaei ; Arizona State University, School for Engineering of Matter, Transport and Energy Kudrawiec, Robert; Wroclaw University of Science and Technology, Department of Semiconductor Materials Engineering Tongay, Sefaattin; Arizona State University, School for Engineering of Matter, Transport and Energy

Pressure-induced suppression of charge density phases across the entire rare-earth tritellurides by optical spectroscopy

Jan Kopaczek[1,2 a)], Han Li[1], Kentaro Yumigeta[1], Renee Sailus[1], Mohammed Y. Sayyad[1], Seyed Tohid Rajaei Moosavy[1], Robert Kudrawiec[2], and Sefaattin Tongay[1a)]

[1]*Materials Science and Engineering, School for Engineering of Matter, Transport and Energy, Arizona State University, Tempe, Arizona 85287, USA*

[2]*Department of Semiconductor Materials Engineering, Faculty of Fundamental Problems of Technology, Wroclaw University of Science and Technology,*

Wybrzeże Wyspiańskiego 27, 50-370 Wrocław, Poland

Abstract

The rare-earth tritellurides (RTe_3) are a distinct class of 2D layered materials that recently gained significant attention due to hosting such quantum collective phenomena as superconductivity or charge density waves (CDW). Many members of this van der Waals (vdW) family crystals exhibit CDW behavior at room temperature, i.e., RTe_3 compound where R=La, Ce, Pr, Nd, Sm, Gd, and Tb. Here, our systematic studies establish the CDW properties of RTe_3 when the vdW spacing/interaction strength between adjacent RTe_3 layers is engineered under extreme hydrostatic pressures. Using a non-destructive spectroscopy technique, pressure-dependent Raman studies first establish the pressure coefficients of phonon and CDW amplitude modes for a variety of RTe_3 materials, including $LaTe_3$, $CeTe_3$, $PrTe_3$, $NdTe_3$, $SmTe_3$, $GdTe_3$, and $TbTe_3$. Results further show that the CDW phase is eventually suppressed at high pressures when the interlayer spacing is reduced and interaction strength is increased. Comparison between different RTe_3 materials shows that $LaTe_3$ with the largest thermodynamic equilibrium interlayer spacing (smallest chemical pressure) exhibits the most stable CDW phases at high pressures. In contrast, CDW phases in late RTe_3 systems with the largest internal chemical pressures are suppressed easily with applied pressure. Overall results provide comprehensive insights into CDW response of the entire RTe_3 series under extreme pressures, offering an understanding of CDW formation/engineering in a unique class of vdW RTe_3 material systems.

[a)] Corresponding authors: jkopacze@asu.edu and sefaattin.tongay@asu.edu

Introduction

Van der Waals (vdW) Rare-Earth Tritellurides (RTe_3) belong to layered material systems with unique quantum collective phenomena, including superconductivity (SC) [1,2] or charge density wave (CDW) formation [3–7] at room temperature. Previously, the interplay between these two states was established for select RTe_3 materials through electrical studies at different temperatures, and pressures. [2] More recent studies have shown the presence of light-induced CDW phase [8], thickness-dependent CDW properties [9], and established GTe_3 as a high carrier mobility material with unique magnetic ordering [10,11]. Lately, much effort has been given to understanding the CDW phase behavior, which is hosted within the Te atomic layers [12] and driven not only by Fermi surface nesting [3] but also by strong electron-phonon interaction [13,14]. Here the two Te layers are separated by the RTe slab, as shown in Figure 1a, and coupled to another RTe_3 stack through van der Waals forces. Studies have shown that using different rare-earth metal cations leads to different CDW temperatures (T_{CDW}) ranging from cryogenic to above room temperature due to different chemical pressures induced within the RTe slabs. [15–17] Considering the correlation between the chemical and

hydrostatic pressures [18], limited electrical and x-ray diffraction studies have reported on CDW phase response under hydrostatic pressure [2,18,19] to engineer their properties.

Here we utilize the non-contact, non-destructive optical techniques (i.e., regular and angle-resolved Raman spectroscopy) and present comprehensive studies across the RTe_3 series to establish the pressure response of vdW CDW RTe_3 systems (where R=La, Ce, Pr, Nd, Sm, Gd, and Tb). The CDW behavior of RTe_3 material under applied pressures was characterized using the Raman spectroscopy technique [1] by analyzing the pressure response of the phonon mode and amplitude mode related to the CDW phase. Studies from 0 to 14.6 GPa established the pressure values at which the CDW state is suppressed for each crystal (P_{CDW}). Based on these studies, our results constructed the phase diagram for RTe_3 systems relating their out-of-plane lattice constant '*b*' with the hydrostatic pressure leading to phase transition from CDW to non-CDW state. Further angle-resolved Raman spectroscopy measurements were performed to elucidate how the vibrational characteristics of the Raman modes change under CDW phase transition at high pressures. Overall results establish the pressure-driven CDW phase suppression for RTe_3 systems using Raman spectroscopy.

Sample synthesis

RTe_3 crystals (Fig.1a-b) were grown by chemical vapor transport (CVT) for R = Nd, Sm, Gd, Tb and self-flux technique for R = La, Ce, Pr. For CVT, one gram of a stoichiometric mixture of rare-earth metal (99.9 %, Alfa Aesar) and tellurium (99.999%. Alfa Aesar) was sealed with 20 mg of iodine (I_2) in a quartz ampoule under vacuum (10^{-5} Torr). The ampoule was heated to the growth temperature ranging from 700 to 840 ^oC depending on rare-earth elements and kept at a constant temperature for a week. Once the growth was completed, the sealed ampoule was controllably cooled down to room temperature over 2 days. For the self-flux technique, 2 grams of a mixture of rare-earth metal and tellurium in the molar ratio R:Te = 3:97 were put in alumina crucibles and sealed together with quartz wool in a quartz ampoule under a vacuum. The ampoule was heated to 700 ^oC over 8 hours and held at that temperature for 8 hours, then cooled to 515 ^oC at the rate of 2 ^oC/h. The decant procedure through centrifugation was performed to remove the flux at 515 ^oC, and then the temperature was reduced to room temperature. The ampoule was opened, and the materials were kept in an inert gas environment to avoid degradation.

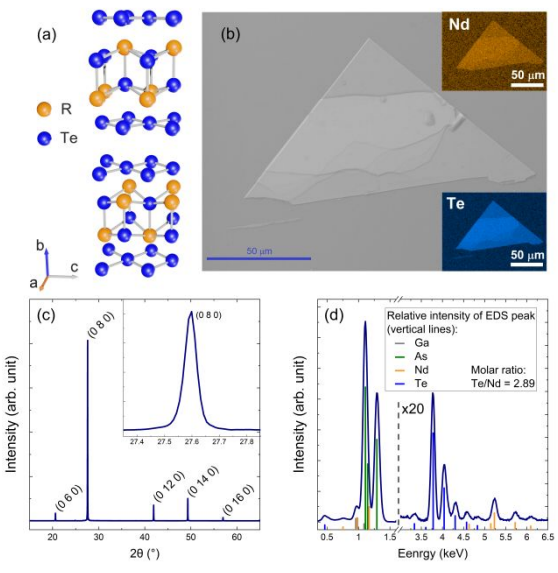

Figure 1 Structural characterization of neodymium tritellurides. (a) Crystal structure of RTe_3 materials which crystalize in the Cmcm space group, (b) SEM images together with EDS compositional maps for Nd and Te elements (inset images). (c) and (d) are respectively XRD and EDS spectra.

The crystallinity of the synthesized crystals was confirmed by x-ray diffraction (XRD) spectroscopy, as shown in Fig. 1c, with a set of distinct and narrow reflections for $NdTe_3$ crystals, which were compared with theoretical predictions as shown in Table S1 in the supporting information (all the other XRD spectra for the RTe_3 were also obtained

by the Malvern PANalytical Aeris system with $Cu_{K\alpha}$ radiation – 1.54056 Å and are shown in Fig. S1). Energy-dispersive x-ray (EDS) mapping (Fig. 1b inset) was performed to confirm the stoichiometry as well as homogenous elemental distribution of lanthanide cations and tellurium anions within the exfoliated vdW sheets. The crystals were exfoliated to yield thin vdW sheets on GaAs substrate, as shown in the scanning electron microscope (SEM) in Fig. 1b (obtained with Zeiss Auriga FIB-SEM).

Experimental methods

For high-pressure studies (up to 14.6 GPa), the RTe_3 crystals were thinned down by mechanical exfoliation using Kapton tape and transferred directly onto the 500 μm culet of the diamond anvil cell (DAC), as depicted in Fig. 2b. As a pressure media, we have used Silicone Oil (AlfaAesar) which does not react chemically with the RTe_3 crystals, remains hydrostatic in the target pressure range, and its Raman signal does not obscure signals from the RTe_3 crystals. For determining the pressure inside the DAC, the position of the diamond Raman mode (1334 cm^{-1}) was tracked. [20] All Raman spectra were obtained in the backscattering configuration with the CW 532nm laser line, where the scattered signal was dispersed by a 0.75 m focal-length Shemrock monochromator. Moreover, the laser beam was focused by a 50x Mitutoyo objective lens to a size of ~5 μm. For angle-resolved Raman spectroscopy (ARRS) measurements, the incident and scattered light were polarized parallelly.

Results and discussion

The pressure-dependent vibrational properties for the vdW RTe_3 crystals can offer unique insight into the CDW phase behavior when the rare earth elements vary across lanthanides. That ordered quantum phenomenon is hosted within the Te sheet of the RTe_3 structure and, at room temperature, is unidirectional (CDW is formed along the c-axis) and incommensurate in nature. [8,21] Prior diffraction studies have shown that the modulation wave vector is similar for each RTe_3 material system [22], and when going from heaviest (Tm) to lightest (La) metal cation, the CDW temperature – the onset temperature for inducing CDW phase transformation – increases from 220 K to above 570 K, marking a change in T_{CDW} as much as ~250 K. [6,17]

For high-pressure studies, we have used DAC (schematically shown in Fig. 2a) together with the Raman setup equipped with the 50x objective lens, where the e-field of the incident and scattered light is parallel to the surface of crystals. This setup allows us to perform micron resolved measurements for mechanically exfoliated thin samples, as shown in Fig. 2b. Based on the factor-group analysis, it was reported that $4A_g + 4B_{1g} + 4B_{3g}$ modes are Raman active. [2,3] Considering our experimental configuration, we could access A_g out of mentioned modes. Nevertheless, B_{1g} modes can also be observed as a result of the layered symmetry of the studied material. [4] Additionally, it was predicted that due to the lattice distortion, B_1 modes should emerge around 84 and 114 cm^{-1}. [2] Because the mode positions in our studies closely resemble those previously reported [2–4], we have tentatively assigned the observed modes as shown in Fig. 2d. The most intense mode observed at around 67 cm^{-1} was identified as an amplitude mode based on its evolution with temperature (detailed analysis was provided in the supporting information Fig. S2). Fig. 2c shows the evolution of $NdTe_3$ Raman spectra from 0 GPa to 13.5 GPa. It can be seen that all modes located above 75 cm^{-1} blueshift with pressure due to lattice stiffening, while their Raman FWHM remains relatively unaffected. Fig. 2c also shows that the intensity of a mode located at 67 cm^{-1} and 84 cm^{-1} decreases, and at around 5 GPa becomes strongly reduced, while 35, 97, and 114 cm^{-1} modes can still be distinguished from the background signal and traced in the entire pressure range. Previous

temperature-dependent Raman studies identified the 67 cm^{-1} mode as the CDW amplitude mode owing to its strong correlation with the CDW response. [3,5] Moreover, as shown in our temperature evolution of Raman spectra (Fig. S2), the mode located at 84 cm^{-1} also exhibits a correlation with the CDW phase. In contrast, 1st order Raman peaks at 35, 97, and 114 cm^{-1} were primarily related to vibrational modes at the Γ=0 in the phonon dispersion curves. [23,24] These Raman spectra were fitted to the Lorentz function at each pressure to obtain frequency and broadening parameters of measured modes, as shown in Fig. 2d. The results of the fitting procedure with Lorentz functions performed for spectra obtained at 0.46 GPa are presented in Fig. S3. Due to the reduced intensity of some of the modes, the uncertainty with which their position was obtained can be significant. For example, at 4.4 GPa, the uncertainty of the position of mode located at around 60 cm^{-1} is comparable to its broadening.

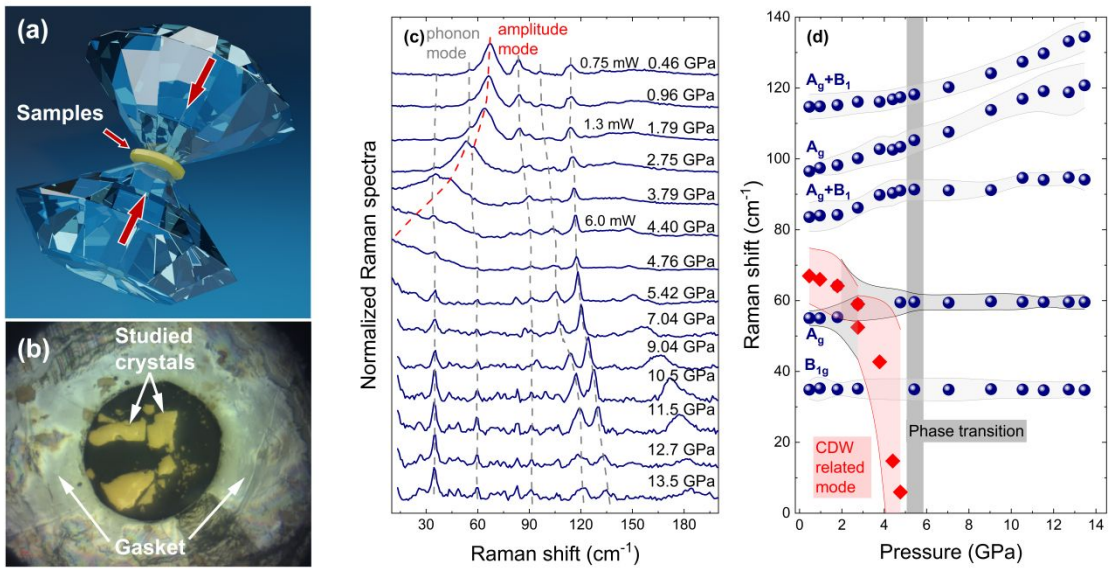

Figure 2 (a) Simplified scheme of DAC and (b) optical image of a sample inside the gasket enclosed within the DAC. (c) Pressure-dependent Raman spectra obtained for $NdTe_3$ crystal (dotted lines are added as an eye guide). (d) Positions of phonon modes (navy spheres) and amplitude (red diamonds) mode in the function of pressure obtained with Lorentz fitting procedure – the shaded area represents broadening of each Raman mode.

The qualitative analysis shows that the pressure coefficient for phonon modes is positive (modes at 97 and 114 cm^{-1}) or negligible (mode at 35 cm^{-1}), i.e., its position does not change with pressure. Furthermore, their broadening (shaded area in Fig. 2d) remains almost constant as well as for most other modes, excluding amplitude modes for which its FWHM increases with pressure from 7 to 45 cm^{-1}. The mode observed at 84 cm^{-1} in the low-pressure range first blueshifts and from 5 GPa becomes less sensitive to changes in pressure, which could suggest its coupling to the CDW phase as indicated by the Raman measurements with temperature. More importantly, the observed behavior of modes at 56 and 67 cm^{-1} reveals the anticrossing interaction of coupled phonon and amplitude modes. At low pressure, the higher branch (at 67 cm^{-1}) has an amplitude nature, whereas the lower branch (at 56 cm^{-1}) is phononic, and at around 2 GPa, the intensities of both modes are comparable, and the natures of both branches reverse. By closely observing the behavior of the lower branch above 2 GPa, the pressure of phase transitions was estimated to be at ~5 GPa, i.e., pressure at which intensity of amplitude mode is not distinguishable from the background signal.

Due to the raw estimation of the $P_{CDW,}$ its value in Fig. 4 was plotted with a large error equal to at least 1 GPa. Here, similar analyses were performed for other RTe_3 crystals (see the supporting information Fig. S4-S6 and Fig. S8-S10), thus creating the library of phase transformations for these

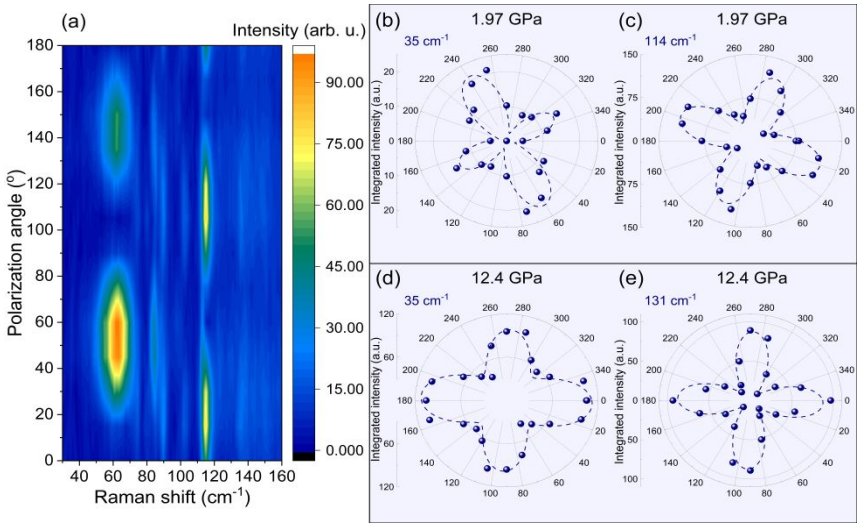

Figure 3 (a) Polarization map of Raman spectra obtained for $NdTe_3$ at 1.97 GPa. The polar plot of the integrated intensity of phonon mode 35 cm^{-1} and 114(131) cm^{-1} obtained at 1.97 GPa (b), (c), and 12.4 GPa (d), (e).

crystal systems.

Angle-resolved Raman measurements were performed to assess how the symmetry of phonon modes changes below and above the CDW phase transition pressure. The results of these studies for $NdTe_3$ crystal are presented in Fig. 3a as an intensity map of Raman signal as a function of the polarization angle where excitation and scattered light were polarized in the parallel direction. The measured angle-resolved phonon modes at 35 and 114 cm^{-1} (~0 GPa) exhibit signature four-fold symmetry as shown in Fig. 3b-c (the complete ARRS data presented in Fig. S11 and Fig. S12). The observed behavior of Raman mode with polarization angle agrees with the results published for $LaTe_3$ crystals, where the distorted structure displays the two-fold and four-fold symmetry of Raman-active modes. [24] Moreover, a similar polarization dependency, i.e., four-fold symmetry, was presented for an amplitude mode studied for $ErTe_3$ crystal. [21] The measured polar plots at 12.4 GPa for 35 cm^{-1} and 131 cm^{-1} modes are presented in Fig. 3d and 3e. We note that their Raman peak positions were tracked starting from 0 GPa to accurately identify/label these modes at low and high pressure, as shown in Fig. 2c by the dotted gray lines. A comparison of ARRS results between 0 vs. 12 GPa implies that the observed four-fold symmetry remains largely unchanged. However, its relative orientation (i.e., polarization orientation) changes possibly due to changes in the Raman tensor caused by the pressure-induced reduction of in-plane lattice constants anisotropy, which arises when CDW is forming. [7,17]

After establishing the pressure-induced suppression of the CDW phase in $NbTe_3$ and other RTe_3 crystals, we propose the phase diagram of RTe_3 CDW behavior across the entire family of RTe_3 systems. Previous studies for $LaTe_3$ and $CeTe_3$ have shown that the satellite XRD peaks corresponding to lattice distortion and evoked by the CDW state will disappear when the volume of the lattice is compressed by 5% [18] offering some insights into pressure-induced effects. In contrast, other Raman studies performed primarily above the critical frequency range (~80 cm^{-1})

prevented observing pressure-induced CDW changes. [24] Here, our comprehensive pressure studies explain how pressure suppresses the CDW state as the *'b'* out-plane lattice constant is varied across the RTe_3 materials system (Fig. 4a) by changing the metal cation type. More specifically, for lighter metal cations such as La in the case of $LaTe_3$, the *'b'* out-of-plane lattice constant is larger (26.27

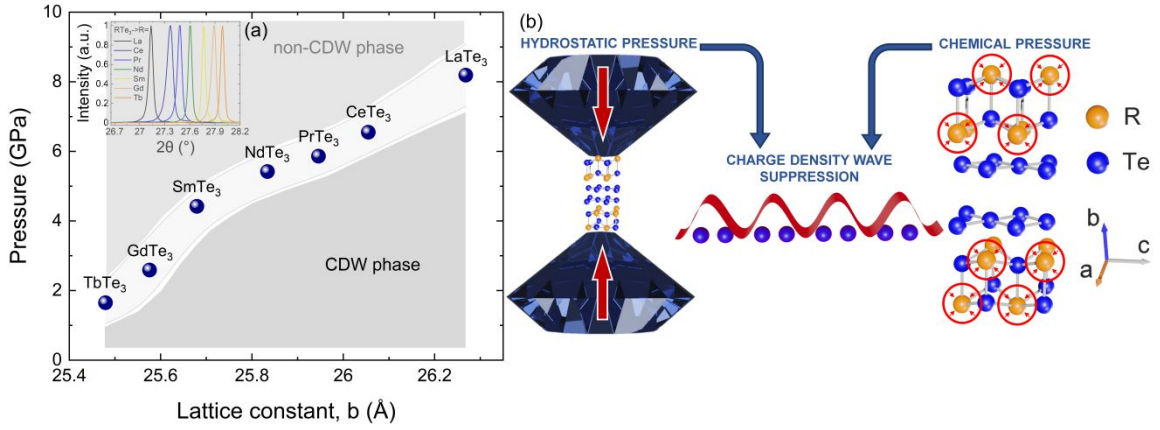

Figure 4 (a) Phase diagram relating pressure at which the CDW diminishes with the out-of-plane lattice constant. The inset represents (080) reflection for XRD spectra across RTe_3 crystals at ambient pressure. (b) Schematic of chemical and hydrostatic pressure equivalence in the RTe_3 material system.

Å) compared to that of the heavier $TbTe_3$ (25.48 Å) vdW crystal. This causes larger in-plane lattice constant anisotropy and higher T_{CDW} moving from Tb to La. [12]

Fig. 4a summarizes the pressure required to cross over from CDW to non-CDW phase across the entire RTe_3 series. The rightmost part of Fig. 4b schematically presents how chemical pressure variation is induced. When the rare-earth element is replaced with a smaller one, the out-of-plane lattice constant (and the unit cell volume) is reduced, causing an increase in chemical pressure. Results in Fig. 4a show that in RTe_3 crystals with large chemical pressure resulting from the smaller lattice constant '*b*' (closer to Tb and away from La), the critical pressure required to induce CDW phase transition is much smaller. In contrast, going from $TbTe_3$ to $LaTe_3$, the chemical pressure is reduced, and the lattice constant '*b*' is increased. Thus, it takes higher hydrostatic pressure to suppress the CDW state. This presents clear evidence for equivalence of chemical and hydrostatic pressure (as shown in Fig. 4b) when the second-order phase transition is considered for RTe_3 materials.

Conclusions

In conclusion, these comprehensive high-pressure studies establish the pressure-induced suppression of CDW phases in vdW RTe_3 systems where R=La, Ce, Pr, Nd, Sm, Gd, and Tb. Results show that the diamond anvil cell integrated with Raman spectroscopy can elucidate CDW behavior in this material system by investigating the Raman active and CDW amplitude modes. Using these methods, we demonstrate that the CDW phase can be easily suppressed by applying hydrostatic pressure for late rare-earth tritellurides (towards $TbTe_3$), whereas significantly larger (>5 times) pressure is required to suppress the CDW phase in early RTe_3 (towards $LaTe_3$). This effect is linked to the already large internal chemical pressure or smaller out-of-plane lattice constant '*b*' in late RTe_3 materials, further confirming the equivalence between hydrostatic and chemical pressures.

Our studies give new insight into the behavior of the CDW phase in vdW RTe_3 crystals and establish the library of pressure responses across the entire RTe_3 material system.

ACKNOWLEDGMENTS

J.K. acknowledges support within the Bekker program from the Polish National Agency for Academic Exchange. S.T acknowledges support from DOE-SC0020653, Applied Materials Inc., NSF CMMI 1825594, NSF DMR-1955889, NSF CMMI-1933214, NSF DMR-1904716, NSF 1935994, and NSF ECCS 2052527 and DMR 2111812.

References

(1) Hamlin, J. J.; Zocco, D. A.; Sayles, T. A.; Maple, M. B.; Chu, J.-H.; Fisher, I. R. Pressure-Induced Superconducting Phase in the Charge-Density-Wave Compound Terbium Tritelluride. *Phys. Rev. Lett.* 2009, *102* (17), 177002. https://doi.org/10.1103/PhysRevLett.102.177002.

(2) Zocco, D. A.; Hamlin, J. J.; Grube, K.; Chu, J.-H.; Kuo, H.-H.; Fisher, I. R.; Maple, M. B. Pressure Dependence of the Charge-Density-Wave and Superconducting States in $GdTe_3$, $TbTe_3$, and $DyTe_3$. *Phys. Rev. B* 2015, *91* (20), 205114. https://doi.org/10.1103/PhysRevB.91.205114.

(3) Brouet, V.; Yang, W. L.; Zhou, X. J.; Hussain, Z.; Ru, N.; Shin, K. Y.; Fisher, I. R.; Shen, Z. X. Fermi Surface Reconstruction in the CDW State of $CeTe_3$ Observed by Photoemission. *Phys. Rev. Lett.* 2004, *93* (12), 126405. https://doi.org/10.1103/PhysRevLett.93.126405.

(4) Brouet, V.; Yang, W. L.; Zhou, X. J.; Hussain, Z.; Moore, R. G.; He, R.; Lu, D. H.; Shen, Z. X.; Laverock, J.; Dugdale, S. B.; Ru, N.; Fisher, I. R. Angle-Resolved Photoemission Study of the Evolution of Band Structure and Charge Density Wave Properties in RTe_3 (R=Y, La, Ce, Sm, Gd, Tb, and Dy). *Phys. Rev. B* 2008, *77* (23), 235104. https://doi.org/10.1103/PhysRevB.77.235104.

(5) Banerjee, A.; Feng, Y.; Silevitch, D. M.; Wang, J.; Lang, J. C.; Kuo, H.-H.; Fisher, I. R.; Rosenbaum, T. F. Charge Transfer and Multiple Density Waves in the Rare Earth Tellurides. *Phys. Rev. B* 2013, *87* (15), 155131. https://doi.org/10.1103/PhysRevB.87.155131.

(6) Hu, B. F.; Cheng, B.; Yuan, R. H.; Dong, T.; Wang, N. L. Coexistence and Competition of Multiple Charge-Density-Wave Orders in Rare-Earth Tritellurides. *Phys. Rev. B* 2014, *90* (8), 085105. https://doi.org/10.1103/PhysRevB.90.085105.

(7) Lazarević, N.; Popović, Z. V.; Hu, R.; Petrovic, C. Evidence of Coupling between Phonons and Charge-Density Waves in $ErTe_3$. *Phys. Rev. B* 2011, *83* (2), 024302. https://doi.org/10.1103/PhysRevB.83.024302.

(8) Kogar, A.; Zong, A.; Dolgirev, P. E.; Shen, X.; Straquadine, J.; Bie, Y.-Q.; Wang, X.; Rohwer, T.; Tung, I.-C.; Yang, Y.; Li, R.; Yang, J.; Weathersby, S.; Park, S.; Kozina, M. E.; Sie, E. J.; Wen, H.; Jarillo-Herrero, P.; Fisher, I. R.; Wang, X.; Gedik, N. Light-Induced Charge Density Wave in LaTe3. *Nat. Phys.* 2020, *16* (2), 159–163. https://doi.org/10.1038/s41567-019-0705-3.

(9) Chen, Y.; Wang, P.; Wu, M.; Ma, J.; Wen, S.; Wu, X.; Li, G.; Zhao, Y.; Wang, K.; Zhang, L.; Huang, L.; Li, W.; Huang, M. Raman Spectra and Dimensional Effect on the Charge Density

Wave Transition in GdTe3. *Appl. Phys. Lett.* 2019, *115* (15), 151905. https://doi.org/10.1063/1.5118870.

(10) Liu, J. S.; Huan, S. C.; Liu, Z. H.; Liu, W. L.; Liu, Z. T.; Lu, X. L.; Huang, Z.; Jiang, Z. C.; Wang, X.; Yu, N.; Zou, Z. Q.; Guo, Y. F.; Shen, D. W. Electronic Structure of the High-Mobility Two-Dimensional Antiferromagnetic Metal $GdTe_3$. *Phys. Rev. Materials* 2020, *4* (11), 114005. https://doi.org/10.1103/PhysRevMaterials.4.114005.

(11) Lei, S.; Lin, J.; Jia, Y.; Gray, M.; Topp, A.; Farahi, G.; Klemenz, S.; Gao, T.; Rodolakis, F.; McChesney, J. L.; Ast, C. R.; Yazdani, A.; Burch, K. S.; Wu, S.; Ong, N. P.; Schoop, L. M. High Mobility in a van Der Waals Layered Antiferromagnetic Metal. *Science Advances 6* (6), eaay6407. https://doi.org/10.1126/sciadv.aay6407.

(12) Yumigeta, K.; Qin, Y.; Li, H.; Blei, M.; Attarde, Y.; Kopas, C.; Tongay, S. Advances in Rare-Earth Tritelluride Quantum Materials: Structure, Properties, and Synthesis. *Advanced Science* 2021, *8* (12), 2004762. https://doi.org/10.1002/advs.202004762.

(13) Johannes, M. D.; Mazin, I. I. Fermi Surface Nesting and the Origin of Charge Density Waves in Metals. *Phys. Rev. B* 2008, *77* (16), 165135. https://doi.org/10.1103/PhysRevB.77.165135.

(14) Lavagnini, M.; Eiter, H.-M.; Tassini, L.; Muschler, B.; Hackl, R.; Monnier, R.; Chu, J.-H.; Fisher, I. R.; Degiorgi, L. Raman Scattering Evidence for a Cascade Evolution of the Charge-Density-Wave Collective Amplitude Mode. *Phys. Rev. B* 2010, *81* (8), 081101. https://doi.org/10.1103/PhysRevB.81.081101.

(15) Phys. Rev. B 52, 14516 (1995) - Chemical pressure and charge-density waves in rare-earth tritellurides https://journals.aps.org/prb/abstract/10.1103/PhysRevB.52.14516.

(16) Sacchetti, A.; Degiorgi, L.; Giamarchi, T.; Ru, N.; Fisher, I. R. Chemical Pressure and Hidden One-Dimensional Behavior in Rare-Earth Tri-Telluride Charge-Density Wave Compounds. *Phys. Rev. B* 2006, *74* (12), 125115. https://doi.org/10.1103/PhysRevB.74.125115.

(17) Ru, N.; Condron, C. L.; Margulis, G. Y.; Shin, K. Y.; Laverock, J.; Dugdale, S. B.; Toney, M. F.; Fisher, I. R. Effect of Chemical Pressure on the Charge Density Wave Transition in Rare-Earth Tritellurides RTe_3. *Phys. Rev. B* 2008, *77* (3), 035114. https://doi.org/10.1103/PhysRevB.77.035114.

(18) Sacchetti, A.; Condron, C. L.; Gvasaliya, S. N.; Pfuner, F.; Lavagnini, M.; Baldini, M.; Toney, M. F.; Merlini, M.; Hanfland, M.; Mesot, J.; Chu, J.-H.; Fisher, I. R.; Postorino, P.; Degiorgi, L. Pressure-Induced Quenching of the Charge-Density-Wave State in Rare-Earth Tritellurides Observed by x-Ray Diffraction. *Phys. Rev. B* 2009, *79* (20), 201101. https://doi.org/10.1103/PhysRevB.79.201101.

(19) Sacchetti, A.; Arcangeletti, E.; Perucchi, A.; Baldassarre, L.; Postorino, P.; Lupi, S.; Ru, N.; Fisher, I. R.; Degiorgi, L. Pressure Dependence of the Charge-Density-Wave Gap in Rare-Earth Tritellurides. *Phys. Rev. Lett.* 2007, *98* (2), 026401. https://doi.org/10.1103/PhysRevLett.98.026401.

(20) Akahama, Y.; Kawamura, H. Pressure Calibration of Diamond Anvil Raman Gauge to 310GPa. *Journal of Applied Physics* 2006, *100* (4), 043516. https://doi.org/10.1063/1.2335683.

(21) Eiter, H.-M.; Lavagnini, M.; Hackl, R.; Nowadnick, E. A.; Kemper, A. F.; Devereaux, T. P.; Chu, J.-H.; Analytis, J. G.; Fisher, I. R.; Degiorgi, L. Alternative Route to Charge Density Wave Formation in Multiband Systems. *PNAS* 2013, *110* (1), 64–69. https://doi.org/10.1073/pnas.1214745110.

(22) Malliakas, C. D.; Kanatzidis, M. G. Divergence in the Behavior of the Charge Density Wave in RETe3 (RE = Rare-Earth Element) with Temperature and RE Element. *J. Am. Chem. Soc.* 2006, *128* (39), 12612–12613. https://doi.org/10.1021/ja0641608.

(23) Kentaro Yumigeta; Attarde, Y.; Jan Kopaczek; Mohammed Y. Sayyad; Yuxia Shen; Mark Blei; Seyed Tohid Rajaei Moosavy; Ying Qin; Sefaattin Tongay. The Phononic and Charge Density Wave Behavior of Entire Rare-Earth Tritelluride Series with Chemical Pressure and Temperature. *Submitted*.

(24) Lavagnini, M.; Baldini, M.; Sacchetti, A.; Di Castro, D.; Delley, B.; Monnier, R.; Chu, J.-H.; Ru, N.; Fisher, I. R.; Postorino, P.; Degiorgi, L. Evidence for Coupling between Charge Density Waves and Phonons in Two-Dimensional Rare-Earth Tritellurides. *Phys. Rev. B* 2008, *78* (20), 201101. https://doi.org/10.1103/PhysRevB.78.201101.